POLITECNICO DI TORINO
Repository ISTITUZIONALE

Stochastic Analysis of Reverse Fault Rupture Hazards in Tunnels Considering Soil Parameter Uncertainties

Original
Stochastic Analysis of Reverse Fault Rupture Hazards in Tunnels Considering Soil Parameter Uncertainties / Mousavi, S.; Noorzad, A.; Ebrahimian, B.; Foti, S.. - In: INTERNATIONAL JOURNAL OF ENGINEERING. TRANSACTIONS A: BASICS. - ISSN 1728-1431. - STAMPA. - 38:4(2025), pp. 744-757. [10.5829/ije.2025.38.04a.07]

Availability:
This version is available at: 11583/3007751 since: 2026-02-18T17:04:46Z

Publisher:
Materials and Energy Research Center

Published
DOI:10.5829/ije.2025.38.04a.07

Terms of use:

This article is made available under terms and conditions as specified in the corresponding bibliographic description in the repository

Publisher copyright

(Article begins on next page)

24 April 2026

IJE TRANSACTIONS A: Basics Vol. 38 No. 04, (April 2025) 744-757

International Journal of Engineering

Journal Homepage: www.ije.ir

Stochastic Analysis of Reverse Fault Rupture Hazards in Tunnels Considering Soil Parameter Uncertainties

S. Mousavi[a], A. Noorzad*[a], B. Ebrahimian[a], S. Foti[b]

[a] *Faculty of Civil, Water and Environmental Engineering Shahid Beheshti University, Iran*
[b] *Department of Structural, Geotechnical and Building Engineering, Politecnico di Torino, Italy*

P A P E R I N F O

Paper history:
Received 22 February 2024
Received in revised form 13 September 2024
Accepted 25 September 2024

Keywords:
Surface Fault Rupture
Stochastic Finite Element Method
Soil Uncertainties
Shallow Tunnels

A B S T R A C T

In an era where underground transportation infrastructure is increasingly vital, the construction of tunnels across fault lines has become a necessary challenge. This study addresses the critical issue of assessing the impact of fault ruptures on shallow tunnels, with a particular emphasis on the variability of soil parameters. We employ the Stochastic Finite Element Method (SFEM), providing a robust framework for simulating the unpredictable nature of soil properties in shallow tunnels under the impacts of surface fault rupture hazards. Our approach highlights the significant influence of soil parameter variations in the analysis of tunnel vulnerability during fault ruptures. The findings offer valuable insights for the design and safety assessment of tunnels in seismically active regions, contributing to the advancement of geotechnical engineering practices in the context of fault rupture hazards. Specifically, the maximum stress values demonstrated substantial increases of 77 and 100% when compared to the 0.5-meter case for the 1.0-meter and 2.0-meter scenarios, respectively.

***doi**: 10.5829/ije.2025.38.04a.07*

Graphical Abstract

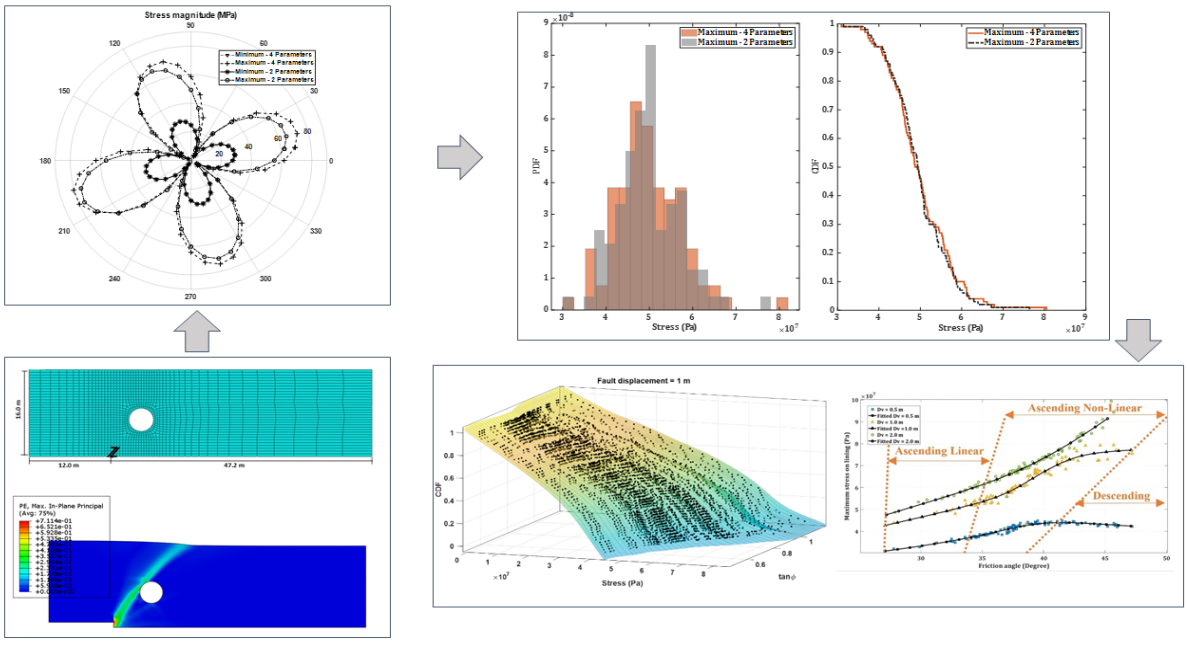

*Corresponding Author Email: a_noorzad@sbu.ac.ir (A. Noorzad)

Please cite this article as: Mousavi S, Noorzad A, Ebrahimian B, Foti S. Stochastic Analysis of Reverse Fault Rupture Hazards in Tunnels Considering Soil Parameter Uncertainties. International Journal of Engineering, Transactions A: Basics. 2025;38(04):744-57.

1. INTRODUCTION

The study of fault rupture impacts on tunnels is crucial, particularly considering past seismic events that have demonstrated the vulnerability of underground structures to surface faulting. Such incidents underscore the need for a deeper understanding of soil behavior during earthquakes and its influence on tunnel integrity. Tunnels, being critical infrastructures, often traverse seismically active zones, making them susceptible to damage from fault movements. The unpredictable nature of fault ruptures, combined with the complex interaction with the surrounding soil, presents a significant challenge for engineers and designers. Hence, researching this area is vital for improving tunnel design, enhancing safety measures, and mitigating the risks associated with seismic activities. This background forms the cornerstone of the motivation behind investigating the impact of fault ruptures on shallow tunnels, particularly considering the uncertainties in soil parameters.

Numerous studies have delved into the phenomenon of fault rupture propagation in soil deposits, including seminal works in experimental simulations (1-7) and several numerical simulation studies (1, 8-12). The damage inflicted by faulting is often severe, presenting considerable challenges for mitigation. Consequently, many standards advocate for fault avoidance strategies.

Prior to the 1999 Chi-Chi earthquake in Taiwan, which registered a moment magnitude (Mw) of 7.6, the phenomenon of faulting was not a primary consideration in the design and construction of structures and infrastructure. However, the extensive surface faulting and resultant damage observed during this earthquake galvanized research into the impacts of faulting (13, 14). Lifelines, such as tunnels, which extend over large distances, frequently intersect with existing faults, making avoidance challenging.

Active research efforts are being directed towards understanding the behavior of lifelines under seismic conditions, as evident in studies by (15-24). Tunnels, as crucial components of infrastructures, have been identified as particularly susceptible to seismic activities. However, focused studies on their seismic behavior are not as extensive. The majority of existing research, which includes both experimental and numerical studies, primarily addresses the behavior of tunnels parallel to fault lines, as highlighted in literature (25-29). Centrifuge tests, conducted by researchers (11, 15, 16, 30), have played a pivotal role in enhancing the understanding of tunnel structures' responses to fault rupture impacts.

This study addresses the critical issue of how fault ruptures impact shallow tunnels, with a particular focus on the uncertainties inherent in soil parameters. The unpredictability of soil behavior under seismic loads, and the complex interactions between soil and structural elements during a fault rupture, necessitate a robust analysis method. The research employs a stochastic finite element method to simulate these interactions, offering a more comprehensive understanding of the risks associated with fault ruptures.

The methodology adopted in this study involves advanced numerical simulations, validated against empirical data from centrifuge tests. The stochastic aspect of the finite element method enables a more realistic representation of the uncertainties associated with soil properties and their impact on tunnel performance during seismic events. This approach not only enhances the predictive accuracy of tunnel behavior during seismic events but also contributes to the development of more resilient underground infrastructure.

2. SURFACE FAULT RUPTURE

Surface rupture is an offset of the ground surface when a fault rupture extends to the Earth's surface. Any structure built across the fault is at risk of being torn apart as the two sides of the fault slip past each other. Surface ruptures can be caused by normal faulting, reverse faulting, or thrust faulting. The form that surface rupturing takes depends on two things: the nature of the material at the surface and the type of fault movement. In seismology, faults are fractures or zones of fractures between two blocks of rock that allow the blocks to move relative to each other.

The probability of a fault rupture reaching the surface during an earthquake depends on several factors, including the magnitude of the earthquake, the nature of geological materials and the type of faulting mechanism involved. According to Lettis et al. (31), the probability of surface rupture for all types of faulting mechanisms increases from approximately 40% at Mw = 5.9 to approximately 90% at Mw = 7.2, and the probability of surface rupture decreases from 40% to 12% at Mw = 5.0.

According to the literature, it is observed that as the earthquake magnitude increases, the fault displacement also increases exponentially. Figure 1 presents a comparison based on three widely used relationships, highlighting how fault displacement varies concerning three distinct earthquake magnitude relationships (32-34). This comparison helps to illustrate and contrast the varying trends predicted by these different relationships regarding fault displacement concerning changes in earthquake magnitude.

3. SURFACE FAULT RUPTURE IMPACTS ON TUNNELS

Surface fault ruptures exert significant and diverse impacts on tunnels (Figure 2 (a & b)). These effects.

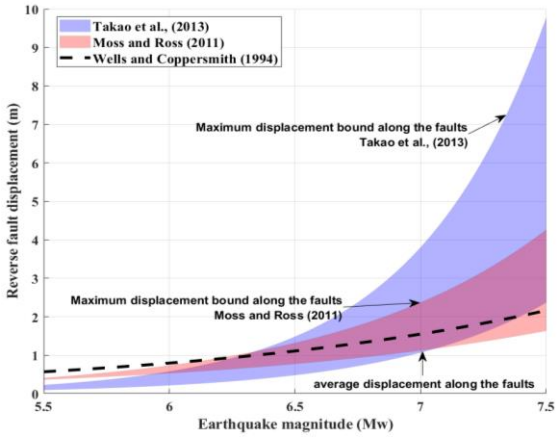

Figure 1. Reverse fault displacement according to earthquake magnitude

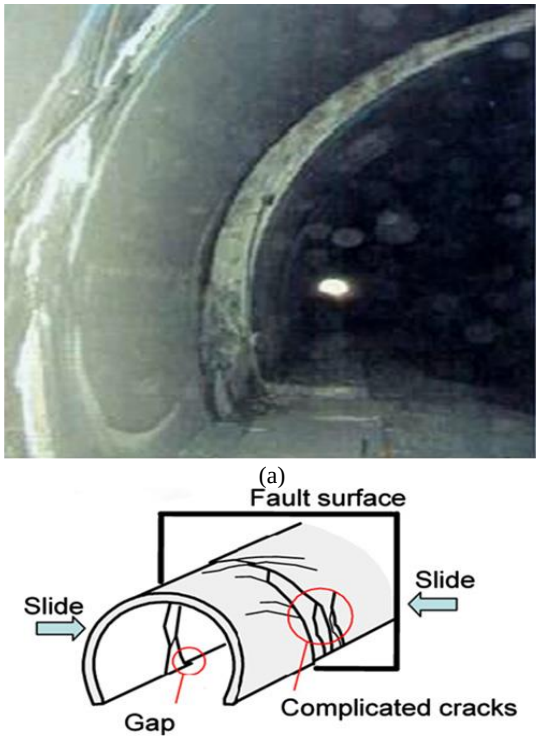

(a)

(b)

Figure 2. (a): Photo from Wenchuan earthquake (30) (b): Damage to tunnels induced by fault rupture (35)

arise from the interaction between seismic activity and tunnel infrastructure. Cracking, deformation, and even partial or complete collapse of tunnel sections can occur. Although shallow tunnels are less affected by extends the fault ruptures, they are still in danger from the surface fault rupture.

A study by Wang and Zhang the repercussions of three seismic events were analyzed, specifically the 1999 Chi-Chi earthquake (Mw 7.3), the 2004 Mid Niigata Prefecture earthquake (Mw 6.8), and the 2008 Wenchuan earthquake (Mw 8.0), on a cohort of 254 tunnels. Their research revealed that 119 of these structures experienced either partial or complete structural failure. Notably, the study determined that not only deep but also shallow tunnels were considerably impacted, with one of the primary sources of damage attributed to deformation due to fault ruptures. The researchers further documented the catastrophic failure of a tunnel as a direct consequence of such deformations. It is clear from the study that the structural integrity of tunnels can be severely compromised by stable displacements stemming from faulting activity.

Infrastructure structures like tunnels typically have recommended allowable displacements falling within the 20-30 mm range, as suggested by different standards (36, 37). However, when exposed to a fault, the displacements experienced by tunnels frequently surpass these prescribed values. This disparity can emerge as a crucial factor impacting both the stability and functionality of tunnels when affected by fault expansion.

4. NUMERICAL MODELING

In this study, the effects of surface fault ruptures on soil and tunnels were investigated by applying the Finite Element Method (FEM). Abaqus 2017 was used to model the fault rupture expansions to the surface and their impacts, and the displacement, stress, strain, and failure modes of the soil and tunnel were examined. The damage and risk of surface fault rupture events were also assessed. Centrifuge test data reported by Baziar et al. (26) were used to validate the numerical models. They tested sand deposits with structures and compared them with FLAC3D models. Good agreement between the experiments and the models was found in terms of fault rupture patterns, displacements, and strains. In this study, we verified our numerical models based on centrifuge tests conducted by Baziar et al. (26, 38).

The analysis herein was conducted under conditions of two-dimensional plane strain, with model dimensions chosen to mirror the prototype scale outlined. The numerical analysis encompassed a two-step process. Initially, the soil profile was subjected to gravitational forces and in-situ stresses, and subsequently solved utilizing the general static solver within Abaqus. The second step involved the quasi-static application of displacements arising from bedrock faulting to the model, accompanied by the implementation of displacement boundary conditions. To ensure model stability and convergence during this phase, faulting displacements were incrementally applied at a controlled rate of less than 5 mm/s. Subsequently, the Dynamic Implicit solver was employed to analyze the model's response to fault occurrence. The soil was represented using CPE4R solid elements, while the lining was modeled with Beam elements (B21). For normal

interaction between the soil and lining, a normal hard contact formulation was utilized, whereas tangential interaction was governed by a tangential penalty equal to 0.4. The geometric configuration of the model is illustrated in Figure 3, and the specific model dimensions are presented in the accompanying Table 1.

Given that the present investigation primarily concerns reverse faulting, the simulation of faulting events involved a static application of footwall faulting and hanging wall faulting, the latter being executed with a controlled displacement rate of less than 5 mm/s. In line with this, the hanging wall was methodically displaced towards the right and upwards to emulate the occurrence of faulting.

The Mohr-Coulomb constitutive model was applied to the soil profile, featuring classical yield criteria, isotropic hardening and softening, a smooth hyperbolic flow potential in the meridional stress plane, and a piecewise elliptic shape in the deviatoric stress plane. Additionally, a linear elastic material model was incorporated to simulate the elastic behaviors. A linear elastic model was applied to the lining that presented the values in Table 2 (16,25,26,39).

In accordance with previous research findings, the fault angle was consistently established at 60 degrees. (11) conducted a comprehensive numerical investigation focusing on the influence of faulting phenomena on shallow tunnel structures. Within their study, they rigorously evaluated tunnel conditions by employing the Demand-Capacity Ratio (DCR) as a key metric (40). Their analysis identified that, regarding both the bending moment and axial force experienced by the tunnel lining, the most critical faulting scenario occurred at an angle of 60 degrees.

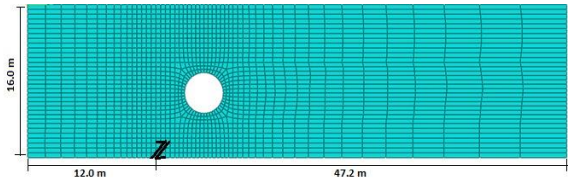

Figure 3. Meshes and dimensions of numerical model

TABLE 1. Dimensions of the numerical model

Geometry	Value
Length of model (m)	59.20
Height of model (m)	16.00
Tunnel diameter (m)	4.24
Lining thickness (m)	0.24
Fault rupture angle (Degree)	60.00

TABLE 2. Lining properties

Geometry	Value
Unit weight (kN/m^3)	24.00
Elastic modulus (GPa)	25.00
Poisson's ratio (-)	0.20

5. DETERMINISTIC NUMERICAL ANALYSIS

5. 1. Fault Rupture Expansion The implementation of displacement-based boundary conditions within the geological stratum comprising the rock bed has engendered a notable stress concentration within the layers of the soil profile proximate to the rock bed. This phenomenon is directly associated with the augmentation of the displacement applied to the bedrock, thereby effectuating greater movement of the hanging wall and subsequently escalating the stress levels imparted onto the underlying soil layers. Consequently, the soil material transitions from an elastic to a plastic state, denoting a shift from regions characterized by reversible deformations to those marked by irreversible deformations.

The prevailing deformation is exacerbated by the accumulation of displacement within the hanging wall, surpassing the allowable limits for soil deformations, while the fault-induced displacements continue to incrementally and quasi-statically intensify. Consequently, this sequential progression gives rise to the initial indications of a shear band formation, primarily manifesting within layers proximal to the bedrock.

With the progressive escalation of displacements and the consequential redistribution of stress into higher stratigraphic layers, the aforementioned shear band advances to elevated regions. This phenomenon, recognized as fault rupture extension, persists until the emergence of a visible surface fault rupture on the terrain's surface. The accompanying Figure 4 visually elucidates the plastic strains resulting from the propagation of the fault to the earth's surface.

Moreover, the presence of a tunnel within this geological context induces significant alterations in the fault's transmission pathway to the surface. In the initial phase, it redirects the fault's trajectory, subsequently

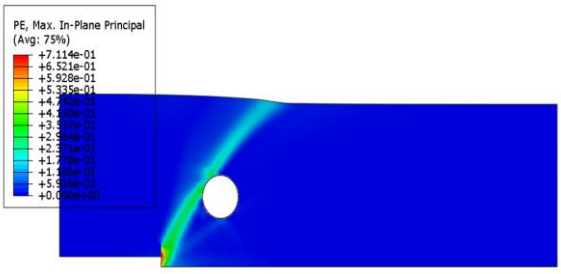

Figure 4. Fault rupture expansion

inducing displacement, deformation, and associated stresses within the tunnel structure during the subsequent phase. In order to evaluate the effects of the fault on the tunnel, we considered the vertical displacement of the fault to be equal to 0.5, 1.0, and 2.0 meters.

5. 2. Displacements on Lining The deformations induced by faulting on the bedrock and their subsequent propagation within the soil profile have given rise to substantial displacements within the tunnel. The magnitude of these displacements exhibits a direct correlation with proximity to the hanging wall and the rupture zone, with regions in proximity experiencing more pronounced displacement and deformation.

As delineated in the provided Figure 5(a), the most considerable displacement, measuring approximately 25 cm, is observed within the angular range of 0-90 degrees in the lining. Conversely, the smallest displacements, approximately 20 cm in magnitude, are localized within the areas spanning 270-0 degrees. It is worth noting that the permissible limit of deformation for tunnel structures can be within the interval of 20-30 mm (37).

5. 3. Stress on the Lining The fault-induced displacements cause stress within the tunnel lining. To conduct a comprehensive examination of the tunnel's response to fault propagation, an investigation into the stress levels within the lining was imperative. In this endeavor, Von Mises stresses were employed within the Abaqus software to assess the stress distribution within the lining. The utilization of Von Mises stress states serves the crucial purpose of elucidating the specific locations and instants where potential yielding or failure within the model may manifest due to the imposed loads and boundary conditions. Figure 5(b) presented herein illustrates the stress magnitudes at various points along the tunnel lining. It is noteworthy that the stress values obtained within the angular range of 180-210 degrees exhibit the highest magnitudes.

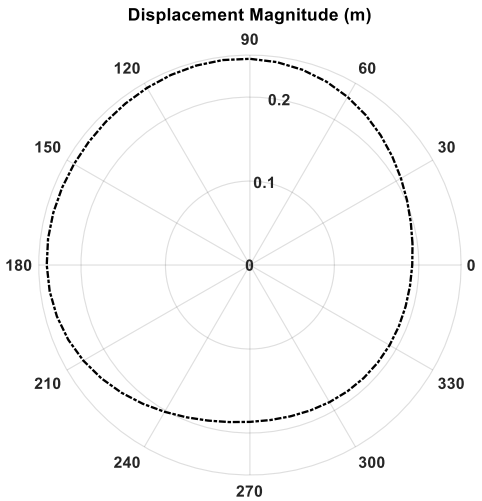

(a)

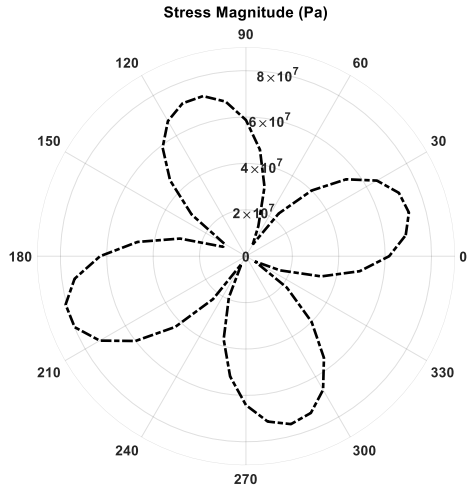

(b)

Figure 5. (a): Displacement on lining (b): Stress on lining

6. STOCHASTIC NUMERICAL ANALYSIS

The use of stochastic numerical analysis is essential for a comprehensive examination of the impacts of surface fault ruptures on shallow tunnels in deposit soils due to the intricate and uncertain nature of earthquake events, the variability in soil properties, uncertainties in fault rupture parameters and ground motion predictions. Probabilistic analysis is crucial for safety assessments, risk quantification, regulatory compliance, and the development of effective mitigation strategies for tunnel infrastructure resilience.

In this paper, to tackle the uncertainties associated with analyzing surface fault rupture hazards in tunnels, we utilize Stochastic Finite Element Analysis (SFEA). The flowchart outlining the analysis procedure, based on SFEA, is depicted in Figure 6. Our focus is on quantifying soil parameter uncertainties, considering the variations in soil properties. This approach aims to provide a more comprehensive assessment of the potential impacts of surface fault ruptures on tunnels, accounting for geotechnical uncertainties. The goal is to improve our understanding of tunnel infrastructure risks and inform decision-making and mitigation strategies.

In pursuit of this objective, and in recognition of the limitations of performing stochastic analysis directly within the Abaqus software, the authors have written a code by developing a custom interface using MATLAB. This interface seamlessly links Abaqus to both the pre-processing and post-processing stages of our models.

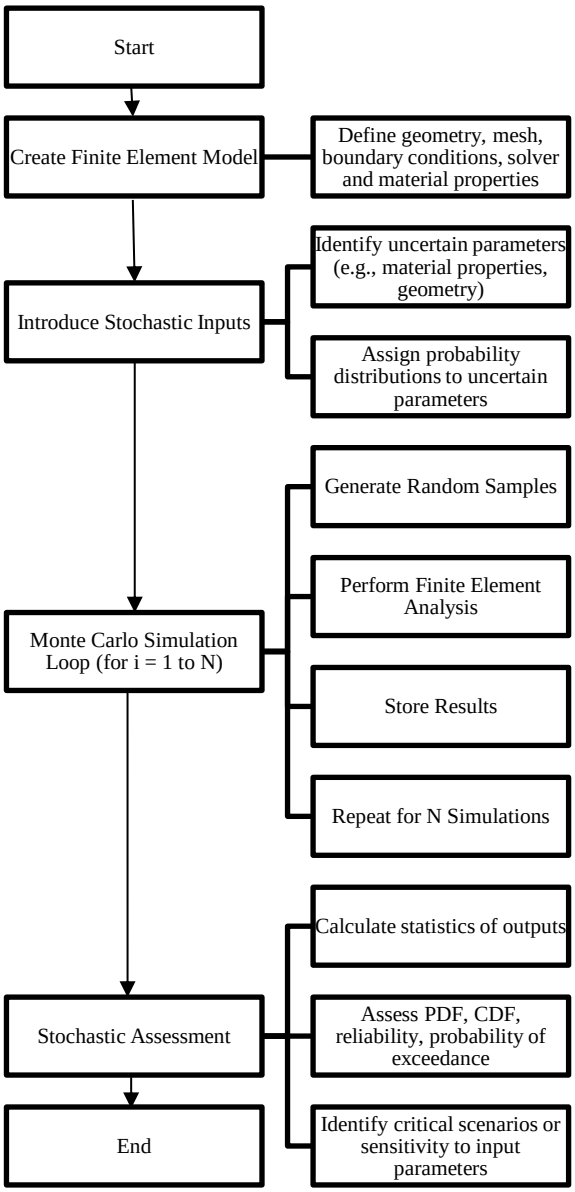

Figure 6. SFEA flowchart

This integrated approach not only overcomes the software limitations but also facilitates a more efficient and accurate execution of the stochastic finite element analysis, enhancing the robustness of our study's findings and the reliability of our risk assessment for tunnel infrastructure subjected to surface fault rupture hazards.

To achieve our research objectives, a multi-step approach was used. Initially, a deterministic model simulated surface fault rupture impacts on tunnels in Abaqus software. The model's input file was then converted into a MATLAB-compatible format to integrate it into MATLAB. MATLAB scripts generated probabilistic distributions for input parameters, incorporating uncertainty. Subsequently, the Abaqus model's input file was updated using these probabilistic values to simulate diverse scenarios reflecting different uncertainties. This iterative process comprehensively assessed potential impacts on tunnel infrastructure by exploring various parameter combinations. Finally, a specialized MATLAB code read and extracted output files from Abaqus simulations. These results were imported into MATLAB for further analysis, enabling a thorough and probabilistic evaluation of surface fault rupture impacts on tunnels with each set of generated probabilistic values (41).

6. 1. Parameter Variability The Mohr-Coulomb constitutive model has been employed as the hardening model in the numerical simulations, while a linear elastic model is utilized as the elastic component. Within this framework, a total of five input parameters must be taken into account: Poisson's ratio, elastic modulus, cohesion, friction angle, and dilation angle. For the specific case of sandy soil, the cohesion parameter was found to be negligible, resulting in a reduction of the effective input parameters to four. To comprehensively explore the impact of uncertainty on these parameters, two distinct types of analyses were conducted. In the first scenario, it was assumed that all four parameters exhibited random behavior, while in the second scenario, specific focus was placed on the random behavior of the hardening parameters, namely, the friction and dilation angles.

These approaches allowed the systematic investigation of the influence of parameter variability on the outcomes of the simulations.

Building upon recommendations from the literature review, numerous researchers emphasized that the normal, truncated normal, and lognormal distributions are more compatible with the behavior of soil parameters (42-49). In this study, the choice was to utilize truncated normal distributions to characterize the variability of input parameters. By considering the stochastic variables within the range of their mean plus or minus four times the standard deviation, 99.99% of the area beneath the normal density curve is covered. The specific values for the normal distribution pertaining to probabilities are outlined in Table 3 within our analysis (50-53).

According to the findings from the literature review (54-56), the correlation coefficient between the friction angle and dilation angle is suggested to be 0.6. This value indicates a moderately positive relationship between these angles in the context of soil mechanics. A correlation coefficient of +0.6 implies that there is a discernible tendency for the friction angle to increase with an increase in the dilation angle, but it's not an absolute relationship. The strength of this correlation suggests a moderate directional association between the two angles, contributing to an understanding of soil behavior during shearing processes.

TABLE 3. Random probabilistic inputs

Parameter	Mean value	Coefficient of variation		Probabilistic distribution
		Two parameters' scenario	Four parameters' scenario	
Elastic modulus (Pa)	25e6	0.0	10%	Normal
Poisson's ratio (-)	0.28	0.0	5%	Normal
Friction angle (Degree)	38	15%	15%	Normal
Dilation angle (Degree)	8	15%	15%	Normal
Number of probabilistic generations		100		

To generate random probabilistic distributions for input parameters, a multi-step process was implemented. Initially, normal distributions were generated for the random parameters while considering the correlation coefficients between each pair of parameters. Subsequently, probabilistic distributions were defined to account for assumed errors, including Measurement errors, Sampling errors, Model errors, and Parameter estimation errors, using normal distributions. In the final step, the summation of errors was added to the initially generated normal distributions. During this step, the assumed correlation coefficients for each pair of parameters were scrutinized. If the specified conditions were met, the generation process concluded; otherwise, the process iterated until the desired criteria were satisfied. This meticulous approach ensured the robust generation of random probabilistic distributions for input parameters, enhancing the reliability of the stochastic analysis.

6. 2. Stochastic Results Understanding the impacts of input parameter deviations can be achieved through stochastic analysis, which differs from deterministic analysis where fixed input values lead to deterministic output values. In stochastic analysis, we calculate distributions for output parameters. This section presents the stochastic results, beginning with a comparison of the scenarios considered.

The methodology employed involves generating N data points for each random input parameter, leading to the calculation of N values for the specific target parameter. For instance, in the case of the i_{th} series of generated random values for inputs parameters, the displacement and stress within the lining were computed. Using random input data from the N series, calculations were performed to determine stress and displacement on the lining. Monte Carlo simulation was employed to derive the PDF for each series. By integrating the area under the PDF curves, the CDF was obtained. Figure 7 displays the inverse CDF (1-CDF) for both displacement and stress on the lining.

A total of 100 input series were taken into consideration, and an analysis was carried out for each of them. Stress calculations for the lining were determined based on the results of each analysis, followed by the calculation of the PDF for stress on the lining. The CDF was subsequently established by utilizing the PDF for each series of stresses on the lining. In this case, it was assumed that the probable earthquake had a magnitude of 6.5 Mw, and based on Figure 1, it was deduced that there was potential for a fault displacement of 1.0 meter. The 1-CDF graph for displacement and stress on the lining for each set of input parameters is presented in Figure 7. From this figure, the probability of stress occurrences on the lining was determined for each set of probabilistic input data distributions.

According to the graphical representation shown in Figure 8(a), it is evident that the maximum and minimum

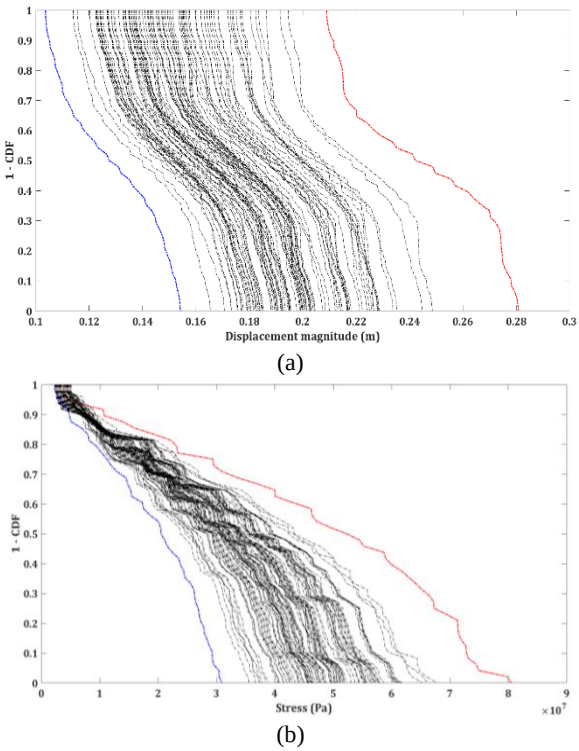

Figure 7. Inverse CDF for (a) displacement and (b) stress on lining

values exhibit similar behaviors in both scenarios mentioned. Specifically, the calculated maximum displacements are 0.281 m for scenarios involving four probabilistic parameters and 0.246 m for scenarios with only two probabilistic parameters. Likewise, the calculated minimum displacements measure 0.1031 m for four probabilistic parameters and 0.1037 m for two probabilistic parameters. These findings highlight that the calculated maximum displacements are approximately 14.0% higher when considering four probabilistic parameters as opposed to two probabilistic parameters. Conversely, the calculated minimum displacements are only about 1.0% lower in scenarios with four probabilistic parameters compared to those with two probabilistic parameters. An illustration in Figure 9(a) showcases a comparison between the PDF and 1-CDF curves representing displacement magnitudes for scenarios involving two and four probabilistic parameters.

This comparison was similarly conducted for stress magnitudes within the lining. Referring to Figure 8(b), it becomes evident that the maximum stress values occur within the 180-210-degree region. Interestingly, the stresses calculated for scenarios involving four probabilistic parameters are approximately 5% higher than those calculated for scenarios involving only two parameters. However, the minimum stress values remain nearly equivalent for both cases mentioned. An illustration in Figure 9(b) showcases a comparison between PDF and CDF curves representing stress magnitudes for scenarios involving two and four probabilistic parameters.

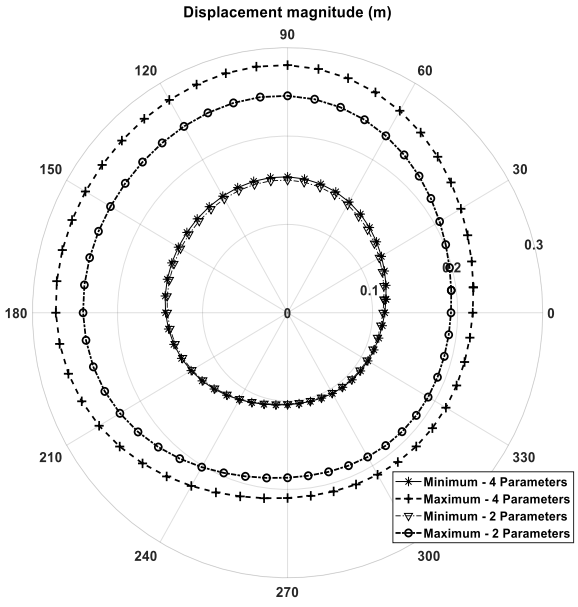

(a)

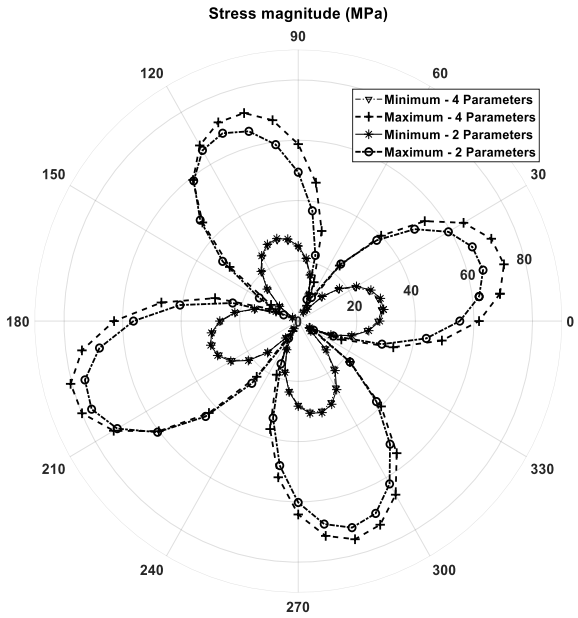

(b)

Figure 8. (a) Maximum and minimum displacement on lining related to 2 and 4 random parameters (b) Maximum and minimum stress on lining related to 2 and 4 random parameters

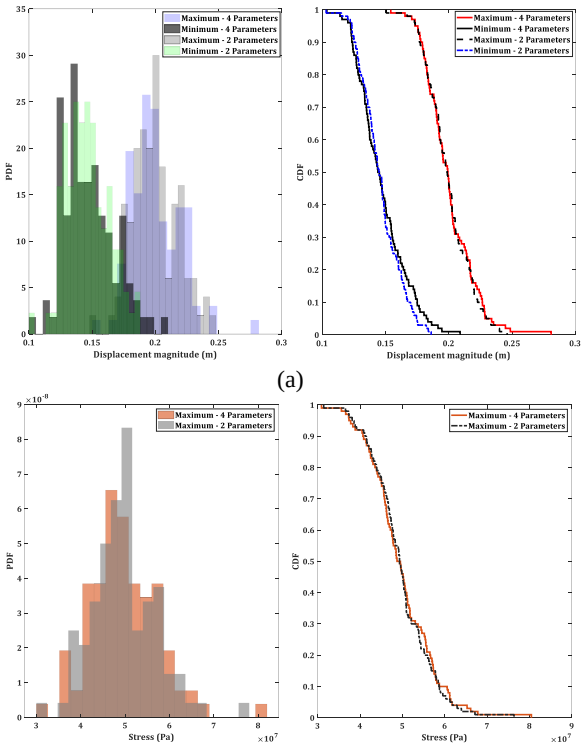

(a)

(b)

Figure 9. (a) PDF and 1-CDF of displacement on lining related to 2 and 4 random parameters (b) PDF and 1-CDF of stress on lining related to 2 and 4 random parameters

As outlined in the preceding section, a clear trend emerges as the number of probabilistic parameters increases, and the calculated maximum values also rise. Conversely, when elastic parameters are introduced into the probabilistic parameter's series, the minimum values are calculated to be lower than those observed in cases with only two probabilistic parameters. This suggests that the range of output variations widens as the number of parameters with variability increases. This suggests that the range of outputs exhibits greater variability as the number of parameters in the analysis increases. It's worth noting that while the influence of elastic parameters may not be substantial, their presence is evident in the altered outcomes. Subsequently, detailed stochastic results for the two parameters' scenarios are presented in the following sections.

Each CDF graph corresponds to a specific series of random input parameters. Upon analyzing the obtained results and graphs, it's apparent that the disparities between the minimum and maximum calculated values are significant. Specifically, in the displacement data, the maximum values appear to be approximately 50% higher than the minimum values. This discrepancy underscores the influence of uncertainties in soil parameters, significantly impacting the outcomes.

6. 3. Zone-Specific Observations Through the investigation of the results, it has been determined that certain zones are identified as the most probable areas for experiencing extreme displacements and stress occurrences. The frequencies of maximum and minimum displacements are displayed in Figure 10(a). It is observed that the maximum and minimum values for horizontal displacements are predominantly found within the ranges of 180-210 degrees and 0-30 degrees, respectively. Additionally, the calculation of displacement magnitude reveals that the maximum values are situated within the zones of 90-120 degrees and 270-300 degrees. The observed trend suggests that the maximum and minimum zones on the lining do not fluctuate or change significantly with variations in soil parameters.

In contrast, stress magnitude exhibits dissimilar behavior compared to displacements. A uniform behavior is not exhibited for stress magnitudes. The maximum stress values are primarily calculated within the ranges of 180-210 degrees and 270-300 degrees, suggesting a higher degree of dependence on variations in soil parameters. Conversely, the minimum stress values are found to be distributed more widely, with frequent occurrences at 330 degrees and occasional instances at 60 and 150 degrees. It is noteworthy that the variability in minimum stress values exceeds that of other calculated parameters, underscoring the significance of these findings.

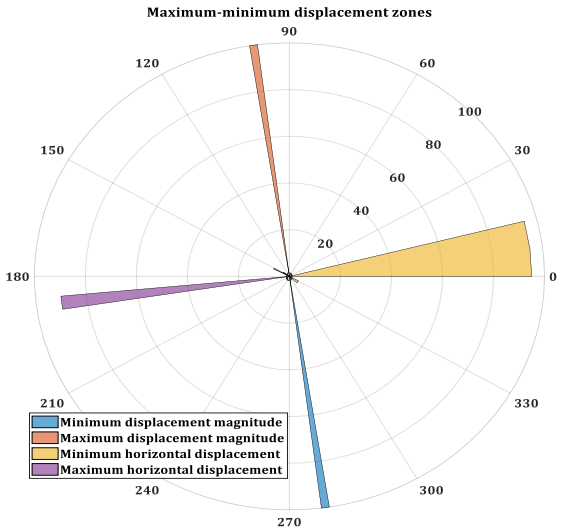

(a)

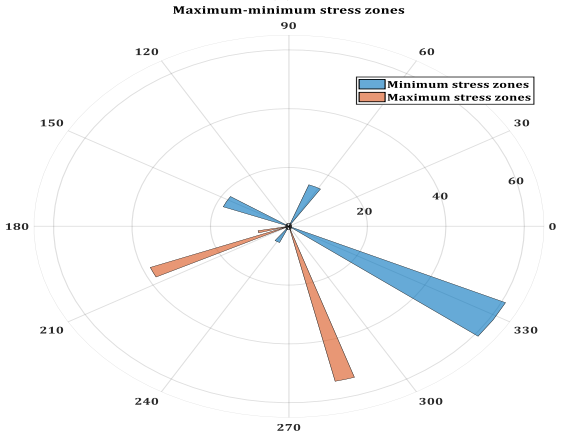

(b)

Figure 10. (a) Maximum and minimum displacement zones on the lining (b) Maximum and minimum stress zones on the lining

6. 4. Considering Soil Parameter Variability As previously noted, for each input parameter set, specifically the dilation angle and friction angle in this context, a total of n generations were considered, resulting in n sets of output parameters, namely, the stress on the lining. Figure 7 visually presents these outcomes in a two-dimensional graph. To assess the influence of soil uncertainty parameters, the third axis is introduced to this graph, and a three-dimensional representation can be constructed, with the friction angle serving as a representative parameter for soil mechanical properties (Figure 11). Within this three-dimensional graph, the respective values for each set of stress on the lining are plotted along the third axis. For enhanced clarity and comprehension, a surface is overlaid onto the graph, intersecting with black points, the calculated values are obtained using SFEA.

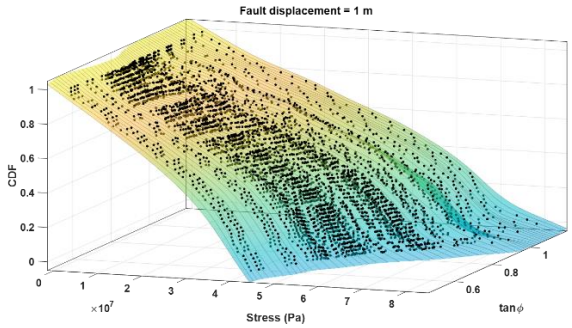

Figure 11. The three-dimensional representation of 1-CDF, friction angle of soil and stress on lining

The analysis process was duplicated for two scenarios, each involving distinct vertical fault rupture displacements. It was assumed that the possible earthquake events could have magnitudes of 6.0, 6.5, and 7.5 Mw. Based on Figure 12, it was deduced that there was potential for fault displacements of 0.5, 1.0, and 2.0 meters. Subsequently, stochastic analysis was conducted for each of these varied vertical fault rupture displacements, resulting in the generation of a separate three-dimensional graph for each case. In Figure 12, these graphs are presented for vertical fault displacements of 0.5 and 2.0 meters.

The 1-CDF graph for the three cases involving vertical fault movements of 0.5, 1.0, and 2.0 meters is depicted in Figure 13. The calculations reveal that the minimum stress values on the lining are approximately equal across these cases, while the maximum stress values exhibit significant differences. Specifically, the maximum stress values are determined as 44.67 MPa, 79.30 MPa, and 89.67 MPa for the 0.5-meter, 1.0-meter, and 2.0-meter vertical fault rupture cases, respectively. This represents a substantial increase of 77.00% and 100.00% when compared to the 0.5-meter case for the 1.0-meter and 2.0-meter scenarios, respectively.

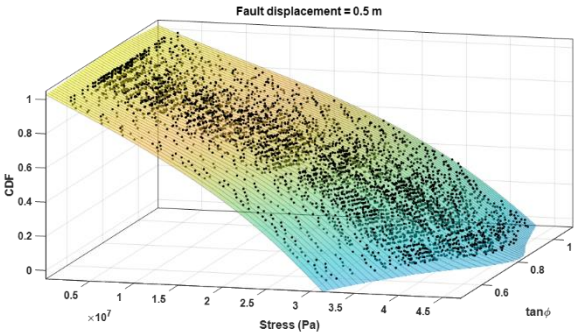

(a)

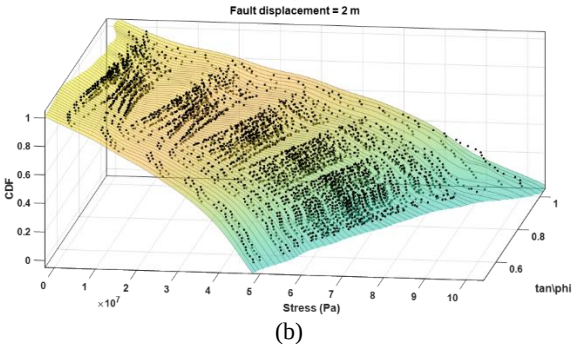

(b)

Figure 12. (a) Three-dimensional graph for fault movement 0.5 m (b) Three-dimensional graph for fault movement 2.0 m

7. PARAMETRIC ANALYSIS

Conducting a statistical analysis utilizing data from fault ruptures of 0.5, 1.0, and 2.0 m in order to establish the range for minimum, maximum, and average stress applied to the lining. The findings are visualized in Figure 14. Within this figure, the minimum ranges appear nearly uniform across all cases, while distinct patterns emerge for both average and maximum stress outcomes. This graph serves as an alternative representation of Figure 13, accomplishing this by omitting the 1-CDF axis. Indeed, based on Figure 14, it appears that as the friction angle values increase, the range of stresses on the lining also increases.

For further clarification, individual graphs were created to represent the maximum values of stresses on the lining for 0.5, 1.0, and 2.0 m fault rupture cases

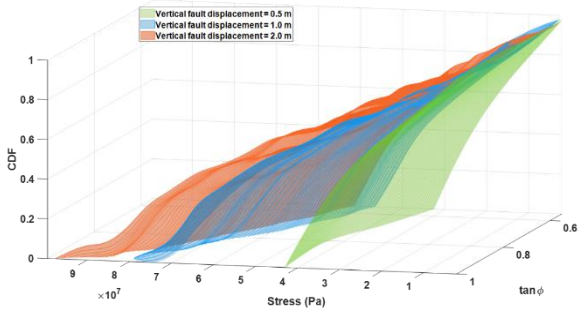

Figure 13. Comparisons of 0.5, 1.0- and 2.0-meters fault movements

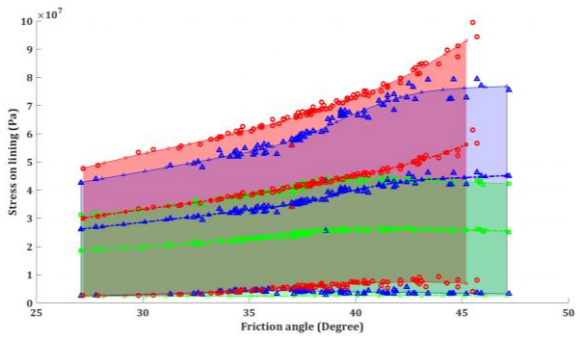

Figure 14. Minimum, maximum, and average stress applied to the lining related to 0.5, 1.0 and 2.0 m fault movements

(Figure 15(a)). Upon analyzing these graphs, it becomes evident that with an increase in fault movements, the stresses on the lining experience a significant elevation. The influence of variations in the friction angle is substantial. As the friction angle increases, the stresses on the lining undergo a primary linear change, followed by a non-linear increase until they reach peak values. In the final phase, the stresses on the lining experience a rare decrease and stabilize within a constant range. These three phases are observed in both the 0.5 and 1.0 m fault movement cases. However, for the 2.0 m case, the first two phases are evident, while the third phase has not yet been reached. Based on the graph, it is apparent that as the value of fault displacements increases, these phases are observed at later stages, particularly in comparison to the case with a 0.5 m fault displacement.

As the fault movements increase, the ascending non-linear region in the graph expands and becomes more prominent, while the descending regions decrease in width. This observation suggests a clear correlation between fault displacement and the behavior of the graph, particularly in the non-linear and descending phases.

In Figure 15(b), the behavior of average stresses on the lining for three different fault rupture displacements is depicted, and these trends are also influenced by variations in the friction angle. It is noteworthy that the behavior of average stresses on the lining mirrors the behavior of maximum stresses. The graph clearly illustrates the presence of the same three distinct phases in the movement of average stresses as seen in the maximum stresses. This further emphasizes the significance of the fault displacement and friction angle in influencing the overall stress levels on the lining.

To simplify the analysis, linear regressions were employed based on the results (Figure 16). These regression lines make the trends more evident and facilitate straightforward comparisons. By utilizing these relationships, it is possible to make rough approximations to comprehend how tunnel lining behaves under the influence of fault ruptures and variations in soil friction angles.

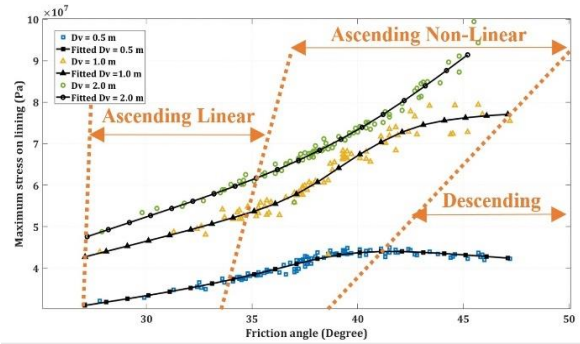

(a)

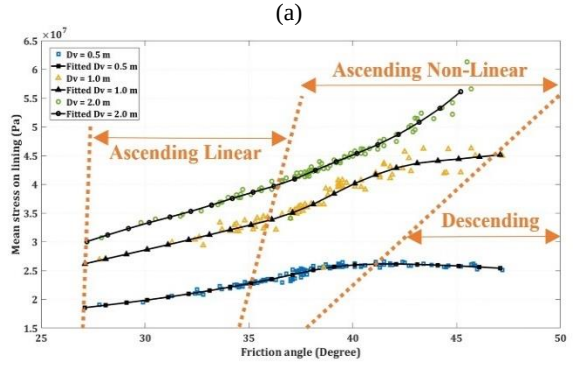

(b)

Figure 15. (a) Maximum stress on lining related to friction angle changes (b) Average stress on lining related to friction angle changes

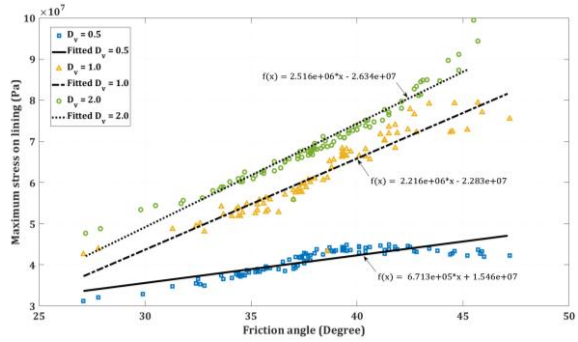

(a)

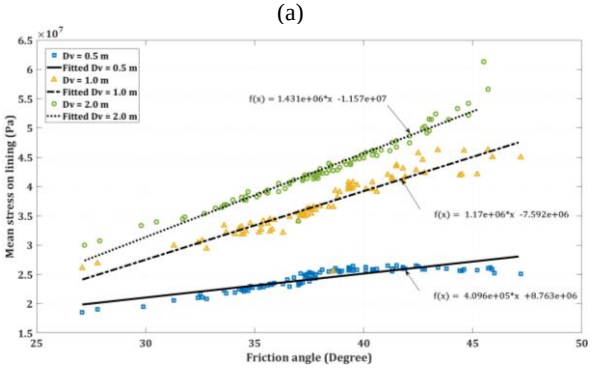

(b)

Figure 16. Linear regressions for maximum stress on lining related to friction angle changes (b): Linear regressions for average stress on lining related to friction angle changes

8. CONCLUSIONS

In conclusion, this study delves into the intricate responses of shallow tunnels when subjected to reverse fault ruptures, with a specific focus on the variability of soil parameters. Employing a rigorous approach, a numerical simulation was executed and validated through comparisons with centrifuge test results gleaned from the existing literature. Recognizing the inherent uncertainties associated with soil properties, our investigation incorporated stochastic analyses to comprehensively

address the unpredictability of soil parameters. A specialized MATLAB-Abaqus interface facilitated the implementation of the stochastic finite element method, with the assumption of normal distributions for uncertainties in input soil parameters.

Sensitivity analyses underscored the significance of considering two plastic parameters, namely the internal friction angle and dilation angle of the soil, in a stochastic manner. This comprehensive approach aimed to enhance the understanding of fault rupture hazards in shallow tunnels. The study postulated potential earthquake events with magnitudes of 6.0, 6.5, and 7.5 Mw, each associated with probable corresponding fault displacements of 0.5, 1.0, and 2.0 meters. Critical parameters for assessing tunnel behavior under fault rupture expansions to the surface were identified as displacements and stresses on the tunnel lining.

Notably, the analysis of displacement magnitudes revealed a consistent trend, indicating relative stability in the maximum and minimum zones on the lining, irrespective of variations in soil parameters. Conversely, stress magnitudes exhibited dissimilar behavior compared to displacements, emphasizing the dependence of zones of concern on soil variability. The study highlighted the soil internal friction angle as a pivotal parameter in explaining soil parameter variability, leading to the presentation of a three-dimensional graph incorporating soil friction angle, fault vertical displacements, and 1-CDF to elucidate tunnel behavior under fault displacement and soil parameter variability.

Further calculations revealed that while minimum stress values on the lining remained approximately constant across the three specified cases, maximum stress values exhibited significant differences. Specifically, the maximum stress values demonstrated substantial increases of 77.00% and 100.00% when compared to the 0.5-meter case for the 1.0-meter and 2.0-meter scenarios, respectively. Parametric analyses unequivocally demonstrated that with an escalation in fault movements, stresses on the lining experienced a significant elevation. The substantial influence of variations in the friction angle was observed, as an increase in the friction angle led to a primary linear change in stresses, followed by a non-linear increase until reaching peak values. In the final phase, stresses on the lining experienced a rare decrease and stabilized within a constant range, highlighting the dynamic interplay of soil parameters and fault rupture hazards in shallow tunnels.

9. REFERENCES

1. Baziar MH, Nabizadeh A, Khalafian N, Lee CJ, Hung WY. Evaluation of reverse faulting effects on the mechanical response of tunnel lining using centrifuge tests and numerical analysis. *Géotechnique*. 2020;70(6):490-502. doi:10.1680/jgeot.18.P.019
2. Bray JD, Seed RB, Cluff LS, Seed HB. Earthquake Fault Rupture Propagation through Soil. *Journal of Geotechnical Engineering*. 1994;120(3):543-561. doi:10.1061/(ASCE)0733-9410(1994)120:3(543)
3. Bray JD, Seed RB, Seed HB. 1 g Small-Scale Modelling of Saturated Cohesive Soils. *Geotechnical Testing Journal*. 1993 Mar 1;16(1):46-53. doi:10.1520/GTJ10266J
4. Cole DA, Lade PV. Influence Zones in Alluvium Over Dip-Slip Faults. *Journal of Geotechnical Engineering*. 1984;110(5):599-615. doi:10.1061/(ASCE)0733-9410(1984)110:5(599)
5. Lee JW, Hamada M. An Experimental Study on Earthquake Fault Rupture Propagation Through a Sandy Soil Deposit. *Structural Engineering / Earthquake Engineering*. 2005;22(1):1s-13s. doi:10.2208/jsceseee.22.1s
6. Sun B, Wang P, Deng M, Liu W, Xu J. Life-cycle dynamic analysis and probabilistic seismic risk assessment of cross-fault hydraulic tunnels considering AAR-induced deterioration. *Soil Dynamics and Earthquake Engineering*. 2024;176:108320. doi:10.1016/j.soildyn.2023.108320
7. Wang T, Geng P, Li P, Wang Q, Wang L. Deformation and failure of overburden soil subjected to normal fault dislocation and its impact on tunnel. *Engineering Failure Analysis*. 2022;142:106747. doi:10.1016/j.engfailanal.2022.106747
8. Chatzidakis D, Tsompanakis Y, Psarropoulos PN. Numerical investigation of secondary-fault rupture propagation through sandy deposits. *Engineering Geology*. 2021;292:106258. doi:10.1016/j.enggeo.2021.106258
9. Garcia FE, Bray JD. Distinct element simulations of earthquake fault rupture through materials of varying density. *Soils and Foundations*. 2018;58(4):986-1000. doi:10.1016/j.sandf.2018.05.009
10. Oettle NK, Bray JD. Numerical Procedures for Simulating Earthquake Fault Rupture Propagation. *International Journal of Geomechanics*. 2017;17(1):04016025. doi:10.1061/(ASCE)GM.1943-5622.0000661
11. Sabagh M, Ghalandarzadeh A. Numerical modelings of continuous shallow tunnels subject to reverse faulting and its verification through a centrifuge. *Computers and Geotechnics*. 2020;128:103813. doi:10.1016/j.compgeo.2020.103813
12. Zhang X, Yu L, Wang M, Yang H. Mechanical response and failure characteristics of tunnels subjected to reverse faulting with nonuniform displacement: Theoretical and numerical investigation. *Engineering Failure Analysis*. 2024;156:107809. doi:10.1016/j.engfailanal.2023.107809
13. Li WH, Lee CH, Ma MH, Huang PJ, Wu SY. Fault Dynamics of the 1999 Chi-Chi earthquake: clues from nanometric geochemical analysis of fault gouges. Scientific Reports. 2019 Apr 5;9(1):5683. doi:10.1038/s41598-019-42028-w
14. Yang H, Beeson J. The Setback Distance Concept and 1999 Chi-Chi (Taiwan) Earthquake. *International Conferences on Recent Advances in Geotechnical Earthquake Engineering and Soil Dynamics*. Published online March 26, 2001. https://scholarsmine.mst.edu/icrageesd/04icrageesd/session10/29
15. Kiani M, Akhlaghi T, Ghalandarzadeh A. Experimental modeling of segmental shallow tunnels in alluvial affected by normal faults. *Tunnelling and Underground Space Technology*. 2016;51:108-119. doi:10.1016/j.tust.2015.10.005
16. Kiani M, Ghalandarzadeh A, Akhlaghi T, Ahmadi M. Experimental evaluation of vulnerability for urban segmental tunnels subjected to normal surface faulting. *Soil Dynamics and Earthquake Engineering*. 2016;89:28-37. doi:10.1016/j.soildyn.2016.07.012
17. Moradi M, Rojhani M, Galandarzadeh A, Takada S. Centrifuge modeling of buried continuous pipelines subjected to normal faulting. Earthquake Engineering and Engineering Vibration. 2013 Mar; 12(1):155-164. doi:10.1007/s11803-013-0159-z

18. Ozturk B. Seismic behavior of two monumental buildings in historical Cappadocia region of Turkey. Bulletin of Earthquake Engineering. 2017 Jul;15:3103-23. doi:10.1007/s10518-016-0082-6
19. Pujol S, Bedirhanoglu I, Donmez C, et al. Quantitative evaluation of the damage to RC buildings caused by the 2023 southeast Turkey earthquake sequence. *Earthquake Spectra*. 2024;40(1):505-530. doi:10.1177/87552930231211208
20. Rashiddel A, Hajihassani M, Kharghani M, Valizadeh H, Rahmannejad R, Dias D. Numerical analysis of segmental tunnel linings - Use of the beam-spring and solid-interface methods. *Geomechanics and Engineering*. 2022;29(4):471-486. doi:10.12989/gae.2022.29.4.471
21. Valizadeh H, Ecemis N. Soil liquefaction-induced uplift of buried pipes in sand-granulated-rubber mixture: Numerical modeling. *Transportation Geotechnics*. 2022;33:100719. doi:10.1016/j.trgeo.2022.100719
22. Yeganeh Khaksar R, Moradi M, Ghalandarzadeh A. Response of buried oil and gas pipelines subjected to reverse faulting: A novel centrifuge-finite element approach. *Scientia Iranica*. 2018;25(5):2501-2516. doi:10.24200/sci.2017.4214
23. Razavian Amrei SA, Mahmoodi M, Ghodrati Amiri GR. Probabilistic Seismic Hazard Assessment of Tehran Based on Arias Intensity. *International Journal of Engineering, Transactions B: Applications*. 2010;23(1):1-20.
24. Baig MA, Ansari MI, Islam N, Umair M. Probabilistic Damage Analysis of Isolated Steel Tub Girder Bridge Excited by Near and Far Fault Ground Motions. *International Journal of Engineering Transactions B: Applications*. 2023;36(2):289-298. doi:10.5829/ije.2023.36.02b.09
25. Azizkandi AS, Ghavami S, Baziar MH, Hasanaklou SH. Assessment of damages in fault rupture–shallow foundation interaction due to the existence of underground structures. *Tunnelling and Underground Space Technology*. 2019;89:222-237. doi:10.1016/j.tust.2019.04.005
26. Baziar MH, Nabizadeh A, Mehrabi R, Lee CJ, Hung WY. Evaluation of underground tunnel response to reverse fault rupture using numerical approach. *Soil Dynamics and Earthquake Engineering*. 2016;83:1-17. doi:10.1016/j.soildyn.2015.11.005
27. Lin ML, Chung CF, Jeng FS, Yao TC. The deformation of overburden soil induced by thrust faulting and its impact on underground tunnels. *Engineering Geology*. 2007;92(3):110-132. doi:10.1016/j.enggeo.2007.03.008
28. Varnusfaderani MG, Golshani A, Majidian S. Analysis of cylindrical tunnels under combined primary near fault seismic excitations and subsequent reverse fault rupture. *Acta Geodynamica et Geromaterialia*. 2017;14(1):5-27.
29. Varnusfaderani MG, Golshani A, Nemati R. Behavior of circular tunnels crossing active faults. *Acta Geodynamica et Geromaterialia*. 2015;12(4):363-377.
30. Baziar MH, Moghadam MR, Kim DS, Choo YW. Effect of underground tunnel on the ground surface acceleration. *Tunnelling and Underground Space Technology*. 2014;44:10-22. doi:10.1016/j.tust.2014.07.004
31. Lettis WR, Wells DL, Baldwin JN. Empirical observations regarding reverse earthquakes, blind thrust faults, and quaternary deformation: Are blind thrust faults truly blind? *Bulletin of the Seismological Society of America*. 1997;87(5):1171-1198. doi:10.1785/BSSA0870051171
32. Moss RES, Ross ZE. Probabilistic Fault Displacement Hazard Analysis for Reverse Faults. *Bulletin of the Seismological Society of America*. 2011;101(4):1542-1553. doi:10.1785/0120100248
33. Takao M, Tsuchiyama J, Annaka T, Kurita T. Application of Probabilistic Fault Displacement Hazard Analysis in Japan. *Journal of Japan Association for Earthquake Engineering*. 2013;13:17-36. doi:10.5610/jaee.13.17
34. Wells DL, Coppersmith KJ. New empirical relationships among magnitude, rupture length, rupture width, rupture area, and surface displacement. *Bulletin of the Seismological Society of America*. 1994;84(4):974-1002. doi:10.1785/BSSA0840040974
35. Miyabayashi H, Iura T, Kojima Y, Yashiro K, Asakura T. Basic Studies on Aseismic Performance of Shallow Mountain Tunnel Lining and It's Seismic Design Method. *Journal of Japan Society of Civil Engineers, Ser F1 (Tunnel Engineering)*. 2011;67:126-143. doi:10.2208/jscejte.67.126
36. ACI PRC-533.5-20: Guide for Precast Concrete Tunnel Segments. Accessed December 18, 2023. https://www.concrete.org/store/productdetail.aspx?ItemID=533520&Language=English&Units=US_Units
37. Eurocode 7: Geotechnical design | Eurocodes: Building the future. Accessed December 18, 2023. https://eurocodes.jrc.ec.europa.eu/EN-Eurocodes/eurocode-7-geotechnical-design
38. Baziar MH, Nabizadeh A, Lee CJ, Hung WY. Centrifuge modeling of interaction between reverse faulting and tunnel. *Soil Dynamics and Earthquake Engineering*. 2014;65:151-164.
39. Cai QP, Peng JM, Ng CharlesWW, Shi JW, Chen XX. Centrifuge and numerical modelling of tunnel intersected by normal fault rupture in sand. *Computers and Geotechnics*. 2019;111:137-146. doi:10.1016/j.compgeo.2019.03.010
40. Hoek E, Carranza-Torres C, Diederichs M, Corkum B. Integration of geotechnical and structural design in tunneling: the 2008 Kersten lecture. In56th Annual Geotechnical Engineering Conference, University of Minnesota, February 2008 Feb 29
41. Papazafeiropoulos G, Muñiz-Calvente M, Martínez-Pañeda E. Abaqus2Matlab: A suitable tool for finite element post-processing. *Advances in Engineering Software*. 2017;105:9-16. doi:10.1016/j.advengsoft.2017.01.006
42. Brejda JJ, Moorman TB, Smith JL, Karlen DL, Allan DL, Dao TH. Distribution and Variability of Surface Soil Properties at a Regional Scale. *Soil Science Society of America Journal*. 2000;64(3):974-982. doi:10.2136/sssaj2000.643974x
43. Fenton GA, Griffiths DV. Bearing-capacity prediction of spatially random c φ soils. Canadian Geotechnical Journal. 2003 Feb 1;40(1):54-65. doi:10.1139/t02-086
44. Johari A, Mousavi S, Hooshmand Nejad A. A seismic slope stability probabilistic model based on Bishop's method using analytical approach. *Scientia Iranica*. 2015;22(3):728-741.
45. Johari A, Mousavi S. An analytical probabilistic analysis of slopes based on limit equilibrium methods. Bulletin of Engineering Geology and the Environment. 2019 Sep 1;78:4333-47. doi:10.1007/s10064-018-1408-1
46. Lumb P. The variability of natural soils. Canadian geotechnical journal. 1966 May 1;3(2):74-97.. doi:10.1139/t66-009
47. Mousavi S, Noorzad A. *Dynamic Reliability Analysis of Earth Dam's Slope Stability*.; 2019.
48. Tobutt DC. Monte Carlo Simulation methods for slope stability. *Computers & Geosciences*. 1982;8(2):199-208. doi:10.1016/0098-3004(82)90021-8
49. Volpe E, Gariano SL, Ciabatta L, Peiro Y, Cattoni E. Expected Changes in Rainfall-Induced Landslide Activity in an Italian Archaeological Area. *Geosciences*. 2023;13(9):270. doi:10.3390/geosciences13090270
50. Dastpak P, Mousavi S, Chenari R, Cami B, Javankhoshdel S. *General Probabilistic Analysis of Simple Reinforced Slopes Using RLEM Approach*.; 2019.
51. Johari A, Momeni M. Stochastic analysis of ground response using non-recursive algorithm. *Soil Dynamics and Earthquake Engineering*. 2015;69:57-82.
52. Johari A, Peiro Y. Determination of stochastic shear strength parameters of a real landslide by back analysis. *International*

Journal of Reliability, Risk and Safety: Theory and Application. 2021;4(1):7-16.

53. Phoon KK. *Reliability-Based Design in Geotechnical Engineering: Computations and Applications*. CRC Press; 2008.
54. Been K, Jefferies MG, Hachey J. The critical state of sands. *Géotechnique*. 1991;41(3):365-381. doi:10.1680/geot.1991.41.3.365
55. Bolton MD. The strength and dilatancy of sands. *Géotechnique*. 1986;36(1):65-78. doi:10.1680/geot.1986.36.1.65
56. Oda M. On Stress-Dilatancy Relation of Sand In Simple Shear Test. *Soils and Foundations*. 1975;15(2):17-29. doi:10.3208/sandf1972.15.2_17

COPYRIGHTS

©2025 The author(s). This is an open access article distributed under the terms of the Creative Commons Attribution (CC BY 4.0), which permits unrestricted use, distribution, and reproduction in any medium, as long as the original authors and source are cited. No permission is required from the authors or the publishers.

Persian Abstract

چکیده

امروزه نیاز به گسترش زیرساخت های حمل و نقل زیرزمینی به یک مسئله حیاتی تبدیل شده است. از سوی دیگر با توجه به کمبود فضاهای زیرزمینی در شهرها، در برخی موارد ساخت تونل‌ها در محل گسل‌ها گریزناپذیر بوده و همین موضوع ممکن است چالش‌های زیادی را نظر ایمنی تونل به همراه داشته باشد. این مطالعه به موضوع حیاتی ارزیابی تأثیر گسیختگی‌های گسل بر تونل‌های کم عمق با تأکید ویژه بر عدم قطعیت پارامترهای خاک می‌پردازد. بدین منظور تلاش شد تا با به‌کارگیری رویکرد جدید المان محدود تصادفی، که چارچوبی قوی برای شبیه‌سازی ماهیت غیرقابل پیش‌بینی خصوصیات خاک در تونل‌های کم‌عمق تحت تأثیر خطرات گسیختگی سطحی ارائه کند. برمبنای تحلیل حساسیت انحام شده دو پارامتر زاویه اصطکاک داخلی و زاویه اتصاع که برای تعریف رفتار غیرخطی خاک استفاده می شوند بعنوان پارامترهای تصادفی در نظر گرفته شده اند. در این مطالعه میزان گسلش متناظر با زلزله های با بزرگای ٦.٠و ٦.٥ و ٧.٠ در نظر گرفته شده است. رویکرد پیشنهادی تأثیر قابل‌توجه تغییرات پارامترهای خاک در تحلیل آسیب‌پذیری تونل در طول گسیختگی گسل را نمایان می سازد. یافته‌ها درک ارزشمندی را برای طراحی و ارزیابی ایمنی تونل‌ها در مناطق لرزه‌ای فعال ارائه می‌دهد که به پیشرفت شیوه‌های مهندسی ژئوتکنیک در زمینه خطرات گسیختگی گسل کمک می‌کند.